Space Sci Rev (2008) 136: 549–563
DOI 10.1007/s11214-007-9255-6

STEREO/Waves Goniopolarimetry

B. Cecconi · X. Bonnin · S. Hoang · M. Maksimovic · S.D. Bale · J.-L. Bougeret · K. Goetz · A. Lecacheux · M.J. Reiner · H.O. Rucker · P. Zarka

Received: 7 December 2006 / Accepted: 25 July 2007 / Published online: 13 October 2007

Abstract The STEREO/Waves experiment is dedicated to the study of inner heliosphere radio emissions. This experiment is composed of a set of two identical receivers placed on each of the two STEREO spacecraft. The STEREO/Waves receivers have instantaneous Goniopolarimetric (GP) capabilities (also referred to as direction-finding capabilities). This means that it is possible to retrieve the direction of arrival of an incoming electromagnetic radio wave, its flux and its polarization. We review the state of the art of GP-capable radio receivers and available GP techniques. We then present the GP capabilities of the STEREO/Waves experiment. We finally show some GP results on solar Type III radio bursts, using data recorded with the Cassini/RPWS/HFR, which are very similar to the STEREO/Waves data.

Keywords STEREO/Waves · Goniopolarimetry (direction finding) · Sun: solar type III bursts

1 Introduction

The STEREO (Solar TErrestrial RElations Observatory) mission (Kaiser 2005) is dedicated to the study of the sun and the inner heliosphere. It is composed of two three-axis stabi-

B. Cecconi (✉) · X. Bonnin · S. Hoang · M. Maksimovic · J.-L. Bougeret · A. Lecacheux · P. Zarka
LESIA, UMR CNRS 8109, Observatoire de Paris, 92195 Meudon, France
e-mail: baptiste.cecconi@obspm.fr

S.D. Bale
Space Sciences Laboratory, Univ. of California, Berkeley, CA 94720, USA

K. Goetz
Dept. of Physics and Astronomy, Univ. of Minnesota, Minneapolis, MN 55455, USA

M.J. Reiner
Hughes STX, Lanham, MD 20706, USA

H.O. Rucker
Space Research Institute, Austrian Academy of Sciences, 8010 Graz, Austria

lized spacecraft orbiting the sun close to the orbit of Earth. The STEREO-A (for "Ahead") spacecraft leads the Earth whereas the STEREO-B (for "Behind") spacecraft trails. The solar longitudinal separation of the two spacecraft is increasing during the mission, as well as their respective distance from the Earth along its orbit. The STEREO/Waves experiment (Bougeret et al. 2007, this issue) is a set of two identical radio receivers placed onboard the two STEREO spacecraft. Both receivers have been developed to fulfill the STEREO mission science objectives and particularly the study of the solar and heliospheric radio emissions: interplanetary (IP) type II radio emission sources, IP shock topology (Hoang et al. 1998; Reiner et al. 1998a); IP type III radio emission sources (Fainberg and Stone 1974); solar wind (SW) radio emission propagation physics (Steinberg et al. 1984; Kellogg 1986).

Inheriting from the High Frequency Receiver of the Radio and Plasma Waves Science (HFR/RPWS) receiver experiment onboard Cassini (Gurnett et al. 2004), the STEREO/Waves receivers have goniopolarimetric (GP) capabilities (also referred to as direction-finding capabilities). That is, the direction of arrival, the polarization state and the flux of the observed electromagnetic wave can be retrieved quasi-instantaneously. As the experiment is deployed on two spacecraft, the localization of the inner heliosphere radio sources through stereoscopic analysis of the GP results is enabled. We will, however, concentrate on the GP capabilities of each receiver independently. The stereoscopic analysis capabilities of the STEREO mission are discussed by Bougeret et al. (2007, this issue).

We review the different GP methods available in the literature in Sect. 2. We then present the GP instrumentation of the STEREO/Waves experiment in Sect. 3. We finally give an insight of the STEREO/Waves capabilities using Cassini/RPWS/HFR data recorded in August 1999, during the Earth flyby.

2 Space-Borne Radio Receivers Goniopolarimetry

Space-borne radio receivers are connected to antennas fulfilling the constraints on size and mass of space missions: i.e., monopole or dipole antennas. These antennas have no intrinsic angular resolution, defined as λ/L, where λ is the wavelength (1 km to 10 m) and L the antenna effective length (typically a few meters); we then have $\lambda/L \sim 1$. A more useful description is their beaming pattern defined as the antenna gain for each direction.

The antenna beaming pattern of a short dipole ($L \ll \lambda$, typically $L \leq 10\lambda$) is proportional to $\sin^2\theta$, where θ is the angular distance from the dipole to the source direction. The frequency range where the antenna is considered as a short dipole is called the quasi-static range or short dipole range. The antenna pattern shows a sharp null in the antenna direction, whereas the maximum gain is obtained for directions perpendicular to the antenna direction. The signal strength measured by a receiver connected to such antennas will thus depend on the orientation of the antenna with respect to the direction of the source. The shape of the beaming pattern implies that it is more efficient to determine the minimum gain than the maximum one. However, the antenna pattern equator can also be detected as the apparent polarization is reversed when crossing this limit. In case of short monopoles (as for Cassini/RPWS or STEREO/Waves), the beaming pattern can be approximated by that of a short dipole. The antenna calibration process provides the effective dipole length and direction equivalent to the system composed of the monopole and the conducting surface of the spacecraft. The antennas used with the STEREO/Waves experiment are described by Bale et al. (2007, this issue).

2.1 Antenna Calibration

The antenna calibration is necessary to get accurate GP results. This calibration provides the length and orientation of the effective electrical dipole equivalent to the electrical system composed of the monopole (or dipole), the antenna mounts and feeds (represented by the antenna and base impedances) (Manning and Fainberg 1980), and the spacecraft body. Three calibration methods are available and complementary: rheometry, electromagnetic simulation and in-flight calibration.

The rheometric analysis is conducted with a scale model of the spacecraft immersed in a tank filled with a dielectric liquid. A low-frequency electric field is applied across the tank and we measure the voltage at the antenna tips while the model spacecraft is slowly rotating (Rucker et al. 1996).

The electromagnetic simulation consists of a computer simulation including a wire grid model of the spacecraft (Fischer et al. 2001; Rucker et al. 2005; Oswald et al. 2006).

In-flight calibrations are conducted using a radio source with known parameters: the jovian HOM (hectometric) emissions has been used to calibrate the effective directions of the Cassini/RPWS antennas, during the Jupiter flyby of Cassini (Vogl et al. 2004; Cecconi and Zarka 2005). The Cassini/RPWS antenna lengths and antenna system gain were calibrated using the galactic background and the system noise data acquired in flight before the antenna deployment (Zarka et al. 2004). The antenna calibrations used for the STEREO/Waves antennas are described thoroughly by Bale et al. (2007, this issue).

2.2 Goniopolarimetric Measurement Expressions

In the quasi-static frequency range, the voltage induced by an incoming electromagnetic wave is $V = \vec{h} \cdot \vec{E}$ where $\vec{h}$ is the effective antenna vector and $\vec{E} = \vec{E}_0 e^{i\omega t}$ is the electric field of the wave. A GP radio receiver then measures a series of correlation values:

$$P_{ij} = \langle V_i V_j^* \rangle, \tag{1}$$

where V_i is the complex voltage measured on the ith antenna, V_j^* is the complex conjugate of the voltage measured on the jth antenna, and $\langle \cdots \rangle$ denotes an average over an integration time longer than the wave period. In the case of an electromagnetic plane wave (i.e., emitted by a point radio source at infinity) characterized by its Stokes parameters (Kraus 1966) (S the flux, Q, U, the linear polarization degrees, and V the circular polarization degree), the voltage correlation can be written as (Cecconi and Zarka 2005):

$$P_{ij} = \frac{Z_0 G h_i h_j S}{2}\left[(1+Q)\Omega_i\Omega_j + (U - iV)\Omega_i\Psi_j + (U + iV)\Omega_j\Psi_i(1-Q)\Psi_i\Psi_j\right], \tag{2}$$

where we have explicitly included the impedance of free space Z_0 and the gain of the antenna system $G h_i h_j$ (Manning and Fainberg 1980); and Ω_i and Ψ_i are the projection of the antenna vector $\vec{h}_i$ on the wave plane axes. When $i = j$, P_{ii} is the autocorrelation of the voltage at the ith antenna outputs, hence a power. When $i \neq j$, P_{ij} is the voltage cross-correlation between the antenna i and j.

Another formalism, proposed by Lecacheux (1978), describes the correlation antenna response with the wave coherence matrix:

$$P_{ij} = {}^t[h_i] \cdot [S] \cdot [h_j]^*, \tag{3}$$

where $[S]$ is the normalized wave coherence matrix that depends on the four Stokes parameters (Lecacheux 1978), ${}^t[h_i]$ is the transpose of $[h_i]$ and $[h_j]^*$ is the complex conjugate of $[h_j]$ ($[h_i]$ and $[h_j]$ being the effective antenna vectors).

As the antenna are measuring the electric field of passing electromagnetic waves in the vicinity of the spacecraft, GP techniques can measure only the direction of the local wave vector. Any propagation effect (such as refraction or diffusion effects) is not taken into account. The directions of arrival obtained with GP techniques only provide apparent sources positions. One should then be particularly careful when analyzing data close to the local plasma frequency where strong refraction can occur on radio waves.

The GP capabilities of a radio receiver depend on the receiver design and especially on the number of independent analysis channels, i.e., the number of simultaneous correlation measurements. For single channel receivers, only one autocorrelation is measured whereas for dual channel receivers (thus connected to two antennas), up to two auto-correlations (one on each antenna) and a complex cross-correlation may be measured. In order to increase the capabilities of the radio receivers (with one or two analysis channels), successive measurements with antenna switching can be performed quasi-instantaneously.

GP techniques are often referred to as direction-finding techniques in the literature. This latter expression does not reflect the fact that these techniques provide both direction and polarization, which are not retrievable independently.

There are two possible ways to achieve GP on space-borne radio receivers: spin demodulation GP (on a spinning spacecraft, like Wind and Ulysses) and instantaneous GP (on three-axis stabilized spacecraft, like Cassini and STEREO). Both of these GP techniques may provide the direction of arrival of the wave, flux, polarization and the angular size of the source. At the time of writing of this paper, inversions providing the size of the source exist for spin demodulation GP, but not for instantaneous GP.

2.3 Spin Demodulation Goniopolarimetry

On a spinning spacecraft, the measured correlation is modulated by the antenna spin. The minimum signal is obtained when the antenna is pointing closest to the source direction. The result of the demodulation is a plane containing the spacecraft spin axis and the source position. This simple method has been used to perform GP analysis of terrestrial Auroral Kilometric Radiation (AKR; Kurth et al. 1975) using the Hawkeye and IMP 8 spacecraft radio data, and of solar type III bursts (Gurnett et al. 1978) using Helios 2, IMP 8 and Hawkeye radio data. The radio receivers used on these spacecraft were single-antenna receivers.

To obtain additional independent measurements, single-channel receivers with antenna switching capabilities were developed for ISEE-3, Wind and Ulysses. These receivers provide series of autocorrelation measurements with different antennas (or antenna combinations) for a given sampling set up (central frequency, integration time, frequency bandwidth).

Lecacheux (1978) proposed GP inversions in the case of (i) one antenna (inclined to the spin axis) and (ii) two antennas (one parallel and one perpendicular to the spin axis). These GP inversions are adapted to the three spacecraft mentioned earlier. GP techniques, including the size of the source, are also available for such receivers (Manning and Fainberg 1980; Fainberg et al. 1985). The techniques developed in these two papers were used to derive the source location of solar radio emissions using (i) ISEE-3 radio data only (Steinberg et al. 1984; Dulk et al. 1986), (ii) Ulysses/URAP data only (Hoang et al. 1994; Reiner et al. 2006), (iii) Wind/Waves data only (Reiner et al. 1998a, 2005) and (iv) Wind/Waves and Ulysses/URAP data performing GP analysis on each data set and then applying triangulation techniques (Hoang et al. 1998; Reiner et al. 1998b, 1998c). These observations are essential to put constraints on the solar radio burst emission mechanism and radio wave propagation.

The GP techniques, as described earlier, have also been applied to the jovian radio emissions observed by Ulysses/URAP during its Jupiter flyby in February 1992 (Reiner et al. 1993; Ladreiter et al. 1994).

The POLRAD experiment on the Interball spacecraft (Hanasz et al. 1998a, 1998b) is a nine-channel receiver connected to three orthogonal electrical dipoles. Each channel of this receiver is outputting a combination of antenna signals (with or without quadrature phase shifts). The full set of GP measurement is thus recorded. GP inversions have been built and used on these data to characterize the AKR (Hanasz et al. 2003; Panchenko 2004).

2.4 Instantaneous Goniopolarimetry

On a spinning spacecraft, no meaningful GP result can be obtained on timescales shorter than the spacecraft spin period. This requires that the wave parameters are fixed over the spin period. Instantaneous measurements require several antennas and multi-channel receivers such as those developed for Cassini/RPWS/HFR and STEREO/Waves. Such receivers provide four independent measurements that can be retrieved instantaneously and seven to nine quasi-instantaneously (Gurnett et al. 2004; Cecconi 2004; Cecconi and Zarka 2005).

For dual-channel receivers, two successive measurements with antenna switching are necessary to obtain the full set of GP unknown (S, Q, U, V, θ and ϕ). We thus have seven independent measurements: P_{ii}, P_{jj}, P_{kk}, $\mathcal{R}e(P_{ij})$, $\mathcal{R}e(P_{ik})$, $\mathcal{I}m(P_{ij})$, $\mathcal{I}m(P_{ik})$ (see (2) for correlation expressions). In case of switching between three antennas, one has nine independent measurements: the seven ones mentioned above plus $\mathcal{R}e(P_{jk})$ and $\mathcal{I}m(P_{jk})$.

The ideal case of an orthogonal triad of antennas was studied by Lecacheux (1978) who showed that measurements on three antennas (i.e., seven or nine measurements) are sufficient to obtain the six wave parameters. It was also mentioned that instantaneous measurements on one pair of antennas (i.e., four measurements) suffice to derive either the source polarization (if the source location is known) or its location (if assumptions on the wave polarization are made).

Due to both geometrical configuration and electromagnetic interaction between the conducting spacecraft body and the antennas, the effective directions of the antennas mounted on spacecraft are generally not orthogonal one to another. GP inversion taking into account a real antenna triad geometry was first proposed by Ladreiter et al. (1995). The proposed GP technique involves a least-square model fitting through singular value decomposition (SVD). A GP inversion using a Powell minimization algorithm was also described by Vogl et al. (2004). Although these methods provide useful estimates on the GP result error, they do not ensure that the provided solution is unique. Another drawback is the computing time needed to invert the data, which is not adequate for long term or large scale automatic processing. In order to overcome these limitations, Cecconi and Zarka (2005) provided analytical inversions to be used on GP data obtained with three antennas.

Ladreiter et al. (1995), Vogl et al. (2004) and Cecconi and Zarka (2005) proposed inversions to perform the antenna calibration needed for accurate GP. In the case of Cassini, the calibration was performed using the Cassini flyby of Jupiter. In the case of S/Waves, spacecraft rolls have been planned at a distance from Earth when AKR can be used as a reference source to calibrate the effective antenna directions.

2.5 Error Sources and Order of Magnitudes

Several sources of error may alter or bias the GP measurements and results. Complete discussions on these sources of error may be found in the papers by Lecacheux (1978), Ladreiter et al. (1995), Cecconi and Zarka (2005) and Cecconi (2007). The different sources of error are the following:

1. *Signal-to-noise ratio.* The signal-to-noise ratio (SNR) is inherent to any measurement. The noise level theoretically depends on the analysis bandwidth b and integration time τ: the signal fluctuations are equal to $S_n/\sqrt{b\tau}$, where S_n is the background level (receiver noise level, interference level, galactic background ...) In theory, this noise interferes only when the signal amplitude is comparable to the noise amplitude. In practice, a SNR larger than 20 to 30 dB is necessary to obtain accurate GP results (Cecconi and Zarka 2005).
2. *Galactic radio background.* In the studied frequency range from <1 MHz to >30 MHz (Dulk et al. 2001), the sky radio background is bright. This background level has to be subtracted from the data before any analysis of GP measurements. The background level has to be determined over a long period of time (Zarka et al. 2004).
3. *Receiver noise.* The receiver noise (mainly from the preamplifier electronics) may be dominant in the low-frequency range (<1 MHz for Cassini). The precise noise level has to be measured onboard the spacecraft, with the receiver power on but before the antenna deployments.
4. *Digitization noise.* When data are digitized as in the case of Cassini or STEREO receivers, they are converted into floating point words of 8 or 12 bits, respectively. Contrary to the SNR fluctuations, which depend on the integration time and frequency bandwidth of observation, the digitization noise is proportional to the signal amplitude (see Fig. 1). The 8 bits digitization superimposes ± 0.17 dB (V^2/Hz) fluctuations on the digitized signal whereas the 12 bits digitization ± 0.04 dB (V^2/Hz) only (Cecconi and Zarka 2005).
5. *Geometrical configuration.* Within the short antenna frequency range, the beaming pattern of an antenna has sharp nulls in the effective antenna direction. This implies that the signal measured on an antenna pointing to the source will be low compared to the case when it is perpendicular to the direction of the source. The SNR of measurements done

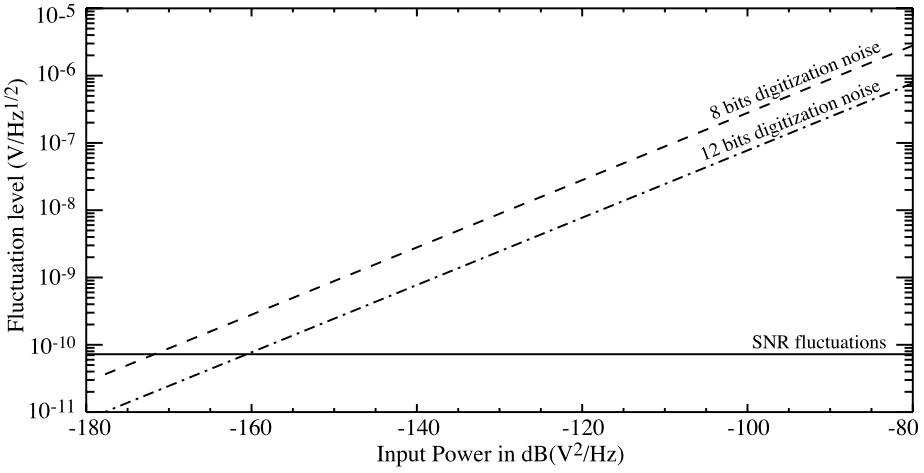

Fig. 1 Simulated noise levels (in $\mathrm{nV \cdot Hz^{-1/2}}$) with respect to input power. *Plain line*: SNR fluctuation level, which is the product of the background level (here fixed to a receiver noise level of 7 $\mathrm{nV \cdot Hz^{-1/2}}$) and the $1/\sqrt{b\tau}$ factor (here fixed to 0.1); *dashed line*: digitization noise (8 bits); *mixed line*: digitization noise (12 bits). For each input power, the *upper line* has to be taken into account to determine the level of noise. The receiver noise level is thus predominant up to input powers of the order of -171 dB (V^2/Hz) for 8 bits digitization (-161 dB (V^2/Hz) for 12 bits)

in such an ill-defined geometrical configuration will then be low. However, as the null is sharp, the direction of arrival of the wave may be obtained accurately (if the antenna system is accurately calibrated), contrary to the flux and polarization measurement.

6. *Inversion indetermination.* Depending on the GP inversion used, series of directions in space or polarization values may not be solved accurately (Cecconi and Zarka 2005). For instance, no valid GP result can be obtained if $V = 0$ in the case of the general GP inversion proposed by Cecconi and Zarka (2005). In that case, another GP inversion was provided.
7. *Calibration indetermination.* Accurate antenna calibration is needed to obtain accurate GP results. Any bias on effective antenna directions will induce offsets on the source location, on the flux and on the polarization degrees obtained with GP inversions (Vogl et al. 2004; Cecconi and Zarka 2005). Two kinds of indetermination may occur: effective antenna length and direction indetermination and misfit to an ideal dipole antenna pattern (especially the warping of the electrical equator for monopole antenna measurements). Current analytical inversions cannot take into account the latter. However, it could be possible to correct for this effect with least square fitting methods.
8. *Intrinsic source variability.* When GP measurements are not recorded simultaneously, source parameters may have changed between two successive measurements. In the case of solar and planetary radio emissions, the flux and the source location are most likely to vary. This source of error is more critical in the case of a spinning spacecraft but it should also be considered on three-axis stabilized spacecraft, when measuring GP samples with antenna switching.
9. *Multiple sources.* The GP inversions proposed in the literature usually suppose a point source or an extended source, but do not take into account the case when several sources are emitting within the antenna pattern at the same frequency. If this happens, the measured power is the sum of the powers induced by each source. If one source dominates by a few orders of magnitude, the GP results will be mainly related to that source. If no source dominates, one should either consider solving the measurement as an extended source (see next point), or develop GP inversions assuming several sources at a time.
10. *Intrinsic size of the source.* When using point source inversions, the case of an extended source (i.e., a resolved source) gives erroneous GP results if the disk-equivalent radius of the source is $>5°$ (Cecconi 2007).

As already mentioned, the direction of arrival provided with GP techniques do not take into account propagation effects that affected the observed radio wave. However, the displacement of the apparent source position due to these propagations effects is not considered to be an indetermination of the GP techniques as there is no way to modify the GP techniques to correct for the distortion of the path of the radio waves between emission and detection.

In order to obtain a typical accuracy of the order of 1° for directions, 10% for polarization degrees, and 1 dB for flux, typical data criteria are: SNR $>$ 23 dB and $\beta_{ij} > 20°$, where β_{ij} is the elevation of the source direction above the plane defined by the ith and jth pair of antennas (Cecconi and Zarka 2005). In practice SNR $>$ 33 dB is necessary to get accurate GP results with the Cassini data. These numbers are valid if the source extension is $<5°$ as seen from the spacecraft (Cecconi 2007). The selection thresholds should be lowered with the S/Waves data, as the digitization noise is there of one order of magnitude smaller.

3 STEREO/Waves Goniopolarimetric Instrumentation

The radio remote sensing part of the experiment consists of three receivers: the Low Frequency Receiver (LFR) covering the 2.5–160 kHz range, the High Frequency Receiver

(HFR) covering the 125 kHz–16 MHz range and the Fixed Frequency Receiver (FFR) providing measurements at 30 or 32 MHz. The high-frequency part of the LFR (10–160 kHz) and the HFR have two simultaneous analysis channels, whereas the low-frequency part of the LFR (2.5–10 kHz) and the FFR have only one. The sensors are a set of three 6 m long electric monopole antennas (Bale et al. 2007, this issue). Each analysis channel can be connected to one of the three antennas (monopole configuration) or to an electrical combination of two of the three antennas (dipole configuration). The antenna connections at the receiver inputs are set by the instrument operating mode. In addition, the operating mode defines the bandwidth and integration time of each measurement as well as the frequency resolution for each receiver. The operating mode (hence the connected antennas) can be changed in-flight as often as necessary.

3.1 Goniopolarimetric Data Samples

Thanks to their two analysis channels, both the LFR (above 10 kHz) and HFR provide GP measurements. The instantaneous measurement used to form the GP data samples consist of a set of four measurements acquired simultaneously using the two connected antennas: two autocorrelations and one complex cross-correlation. This set of four real measurements is called a GP0 data sample. A GP data sample can be composed of a set of either one, two or three GP0 data samples, obtained with antenna switching at the receiver inputs between successive GP0 measurements.

A GP1 data sample is composed of eight measurements (two successive GP0 data samples with antenna switching). We then obtain four auto-correlations and two complex cross-correlations. As one of the two antennas remain the same during the antenna switching two of the four autocorrelations are measured on the same antenna. Although we keep these two redundant autocorrelations as a check for emission stationarity, we actually get seven independent measurements.

A GP2 data sample is composed of 12 measurements (three successive GP0 data samples with antenna switching). Each of the GP0 measurements is made with a different pair of antenna. We obtain six auto-correlations (with redundancy: two autocorrelations on each antenna, i.e. only three independent measurements) and three complex cross-correlations. The three redundant auto-correlations are kept for emission stationarity check. We thus get nine independent measurements.

The GP unknowns are the wave direction of arrival (opposite to the direction of the wave vector $\vec{k}$ and usually represented using two angles: the colatitude θ and the azimuth ϕ), the wave flux and polarization state (usually represented by the four wave Stokes parameters: the intensity S, the degree of circular polarization V and the two linear polarization degrees U and Q), and the source size [represented by its disk-equivalent radius γ (Cecconi 2007)]. We then have seven unknowns. The correlation measurements can be expressed in terms of these GP unknowns and of the antenna parameters: three parameters for each antenna (effective length, colatitude and azimuth of the antenna direction). The set of equations linking the four (GP0), seven (GP1) or nine (GP2) independent measurements to the GP unknowns and antenna parameters is called the GP system of equations. As mentioned by Cecconi and Zarka (2005), there is an intrinsic indetermination within the GP system of equations: two waves with opposite direction of arrival and opposite circular polarization degree will give the exact same response on the antenna. This means that the GP system of equations is degenerate and that the GP1 data samples do not provide enough independent measurements to solve for the seven GP unknowns. The GP2 data samples will provide enough measurements to achieve the inversion for the whole set of GP unknowns. The GP1

data samples may still be used to obtain part of the GP unknowns, assuming some of them to be known.

3.2 Adapted Goniopolarimetric Equations

In the case of type II and III solar bursts, we can assume that the emission is not polarized in the S/Waves frequency range and that source is extended. We can then set Q, U and V to zero and solve for the four remaining unknowns (S, θ, ϕ, γ). According to (33) in Cecconi (2007), the measurement expression is then:

$$P_{ij} = \frac{Z_0\, Gh_i h_j\, S}{4}\left[(A_i A_j + B_i B_j)\left(\Gamma_1 + \frac{\Gamma_1+\Gamma_3}{4}\right) + 2C_i C_j\left(\Gamma_1 - \frac{\Gamma_1+\Gamma_3}{4}\right)\right], \quad (4)$$

where Z_0 is the impedance of free space, $Gh_i h_j$ the gain of the antenna system (Manning and Fainberg 1980), S the flux density,

$$A_i = -\sin\theta_i \cos\theta_c \cos(\phi_c - \phi_i) + \cos\theta_i \sin\theta_c, \quad (5)$$

$$B_i = -\sin\theta_i \sin(\phi_c - \phi_i), \quad (6)$$

$$C_i = \sin\theta_i \sin\theta_c \cos(\phi_c - \phi_i) + \cos\theta_i \cos\theta_c \quad (7)$$

with (θ_c,ϕ_c) the direction of the source centroid, and (θ_i,ϕ_i) the direction of the ith antenna, and Γ_k are the coefficients depending on the brightness distribution and the size of the source. In case of an uniform source, we have $\Gamma_1 = 1$ and $\Gamma_3 = \frac{4}{3}(1+\cos\gamma+\cos^2\gamma)-1$, with γ the disk-equivalent radius of the source (Cecconi 2007). As the source is assumed unpolarized, the imaginary part of the cross-correlation is zero. A GP0 data set provides then only three measurements, which is not enough to solve for the four remaining unknowns.

4 Application of Goniopolarimetry to the Study of Solar Type III Radio Bursts

As mentioned earlier, the GP capabilities of the S/Waves receivers are very similar to those from the Cassini/RPWS/HFR experiment, although only GP0 and GP1 data samples are available with Cassini. We present here an illustration of GP results for a type III solar radio bursts observed during the Cassini Earth flyby in August–September 1999. These results give an overall view of what we expect to measure with the S/Waves radio instrument. Simultaneous GP results obtained with the Wind radio receiver are also shown for comparison.

Cassini GP results were obtained using a direct inversion method applied to GP0 data with Stokes parameters Q, U set to zero (these assumptions do not affect type III burst GP results since type III bursts are known to be linearly unpolarized below 20 MHz due to propagation effects). This allows us to retrieve the remaining unknowns (S, V, θ, ϕ) for each measurements (Cecconi and Zarka 2005). GP measurements taking into account a finite angular radius γ of the source are not illustrated here, but they will be considered with upcoming S/Waves data (Cecconi 2007).

Solar type III radio bursts are produced by beams of suprathermal electrons ($v \sim 0.03$ to $0.3c$) accelerated from active regions (AR) and traveling outward along open magnetic field lines to lower densities n_e in the interplanetary medium (IPM). Along their path in the IPM, these electrons trigger intense Langmuir waves which are partly converted into radio emission at the fundamental (F) and/or second harmonic (H) of the local plasma frequency f_p. Since $f_p \propto \sqrt{n_e}$ and $n_e \propto 1/r^2$ (n_e is the plasma density and r the distance to sun),

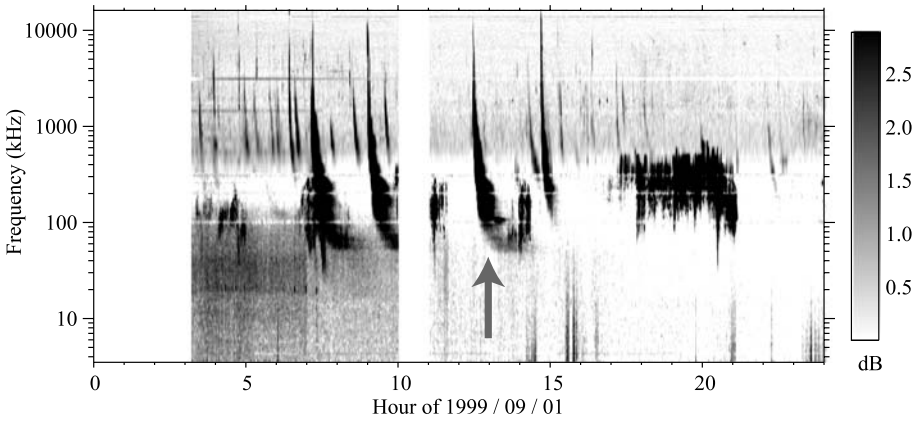

Fig. 2 Cassini/RPWS dynamic spectrum on September 1, 1999. Several type III bursts are visible as well as AKR. The selected event was observed between ∼12:25 and ∼14:30 UT (marked by the *grey arrow*). The event becomes noisy below ∼100 kHz due to possible pollution from AKR

$f_p \propto 1/r$. The heliocentric distances of the type III radio sources thus increase as their frequency decreases.

To illustrate the GP capabilities onboard a three-axis stabilized spacecraft, we have chosen an isolated type III burst observed by Cassini during the Earth flyby. Figure 2 displays a Cassini/RPWS/HFR dynamic spectrum on September 1, 1999. Cassini was at ∼1.13 AU from the Sun. Its Heliocentric Earth Ecliptic (HEE) latitude and longitude were, respectively, ∼+1°N and ∼+1°W. Several type III bursts were observed this day. The selected type III burst occurred between 12:25 UT (at $f \sim 10$ MHz) and 14:30 UT (at $f \sim 40$ kHz). It was associated with NOAA AR 8681 observed at HEE coordinates (+25°N, +28°W) using Nancay Radioheliograph observations at 327 and 164 MHz (obtained from the http://secchirh.obspm.frserver). No flare was observed at this time, however. Data points with SNR above 20 dB and in the frequency range [100–1025 kHz] have been selected. The signal is noisy below 100 kHz due to possible pollution from AKR. Some data points have also been removed due to interference lines.

The GP results corresponding to the selected burst are shown in Fig. 3. Plot (a) represents the average distance in units of a solar radius ($R_\odot$) from the Sun to the source centroid direction as referred to the Sun–Cassini line as a function of frequency. The plot clearly shows that the distance increases with decreasing frequencies, which means that the type III source moves away from the sun with time. Plots (b) and (c) represent, respectively, the average E–W elongation and S–N elevation in solar radius of the source direction relative to the Sun–spacecraft line as functions of frequency. We can see the type III source moving north (from ∼20 $R_\odot$ at 1,000 kHz to ∼120 $R_\odot$ at 100 kHz), with an elongation close to the Sun–spacecraft direction. The standard deviation of the measured distribution are given on the plots. The error bars are noticeably larger at low frequencies. This is due to the fact that the low-frequency range (<320 kHz) is sampled with a theoretical normalized noise $(B\tau)^{-1/2} = 0.066$ whereas the high-frequency range (>320 kHz) with $(B\tau)^{-1/2} = 0.035$, where B and τ are, respectively, the effective bandwidth and integration time of the measurements.

According to the AR's location, these GP results are compatible with a type III electron beam moving along Archimedean spiral-like magnetic field lines. However we can formulate two remarks: (i) this event is atypical since the type III sources follow open magnetic

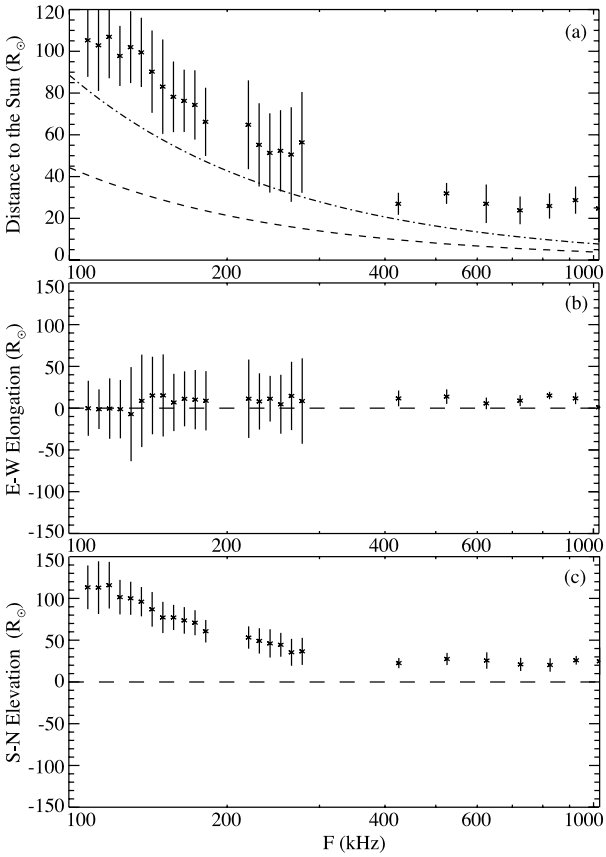

Fig. 3 RPWS/HFR GP results of solar type III radio burst observed by Cassini between 12:25 and 14:30 UT on September 1, 1999. Plot (**a**) represents distance r in solar radius ($R_\odot$) between the center of the Sun and apparent source direction as seen from the spacecraft (i.e., $r = r_c \sin\alpha$, where $r_c = 1$ AU ~ 214 $R_\odot$ and α is the angular distance from the Sun to the source location as seen from the spacecraft). The *dashed* and *mixed lines* give the distance from the sun deduced from a simple density model for the F and H components, respectively. Plots (**b**) and (**c**) represent, respectively, source elongation and elevation in solar radius in the coordinate system centered on the spacecraft and aligned with the spacecraft–Sun direction

field lines which are more usually localized around the solar equatorial plane. (ii) Using a simple IPM density model where the electron density decreases approximately as $\sim 1/r^2$, and assuming fundamental (F) emission at f_p, we expect to measure the burst position at ~ 4 $R_\odot$ at 1,000 kHz and at ~ 40 $R_\odot$ at 100 kHz. This means that the burst position measured by GP is about two to five times farther than the location inferred from a simple density model. There are two possible explanations for this effect. On the one hand, we may observe the second harmonic component which radiates at $2f_p$, or also a mix of both, F and H, components (for more details see Dulk et al. 1984). For instance, the emission measured at 100 kHz should come, in this case, from a location where $f_p \sim 50$ kHz which corresponds to a distance of ~ 84 $R_\odot$, as suggested by the curves in Fig. 3a and Fig. 4a. On the other hand, important scattering effects exist in the IPM and may strongly affect the radio emissions propagation especially close to the source at the fundamental (Steinberg et al. 1984). In all the cases, the only knowledge of the GP measurements is not sufficient to solve this issue. It requires more thorough investigations about the propagation effects and the F/H components determination which is not the purpose of this paper.

The same event was simultaneously observed by the Wind/Waves/RAD2 and RAD1 receivers. At this time, Wind was at ~ 1 AU beyond the Earth's bow shock. The angular elongation distance between the two spacecraft was $\sim 1°$ as seen from the Sun. This does not allow event localization using triangulation methods. GP measurements available on WAVES/RAD1 (20–1,040 kHz) were obtained using a non-linear sweeping

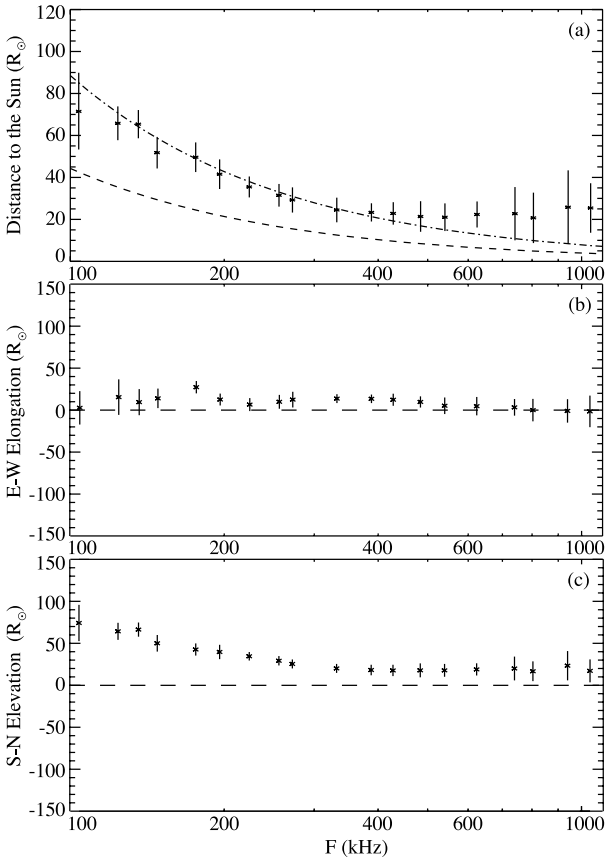

Fig. 4 Waves/RAD1 GP results of solar type III radio burst observed by Wind between 12:25 and 14:30 UT on September 1, 1999. Plot (**a**) represents distance r in units of solar radii ($R_\odot$) between the center of the Sun and apparent source direction as seen from the spacecraft (i.e., $r = r_c \sin\alpha$, where $r_c = 1$ AU $\sim 214\ R_\odot$ and α is the angular distance from the Sun to the source location as seen from the spacecraft). The *dashed* and *mixed lines* give the distance from the Sun deduced from a simple density model, respectively, for the F and H components. Plots (**b**) and (**c**) represent respectively source elongation and elevation in units of solar radii in the coordinate system frame centered on the spacecraft and aligned with the spacecraft–Sun direction

mode which is well suited to type III observations. In this mode, 32 frequency channels are selected among the 256 possibilities in such a way that sampling rate increases with frequency. At each frequency, the signal is sampled during about one spin period ($\sim$3 sec), and it takes about three minutes to obtain a complete 32-frequency sweep. The unknowns (θ, ϕ, γ) are then deduced from GP analysis (Manning and Fainberg 1980; Fainberg et al. 1985).

Figure 4 shows GP measurements for the same type III burst observed by Wind. Assuming that each GP direction of arrival result (θ, ϕ) is the centroid of a Gaussian source distribution, plots (a), (b) and (c) are equivalent to those for Cassini. Figure 5 summarizes the GP observations by the two spacecraft. This figure clearly emphasizes that the GP results from both spacecraft are consistent. Figure 6 represents the average angular radius of the source as a function of the frequency. This latter plot shows that apparent source size increases significantly with decreasing frequency ($\lesssim 20°$ at 1 MHz to $>50°$ at 100 kHz).

As the Cassini data have been treated with a point source GP inversion, the GP results are biases. We simulated the GP results that would output the Cassini radio receiver with an extended source having the parameters found by the Wind at the lower frequency channel (E–W elongation $\sim$0 $R_\odot$, N–S elevation $\sim$70 $R_\odot$ with a angular extension of 50°). We obtain an apparent source shifted northward by $\sim 11°$, which gives an N–S elevation of the order of 110 $R_\odot$, which is exactly what we get with Cassini on the real data. So, despite a wide source extension implying strong biases on the Cassini results, the GP results on both

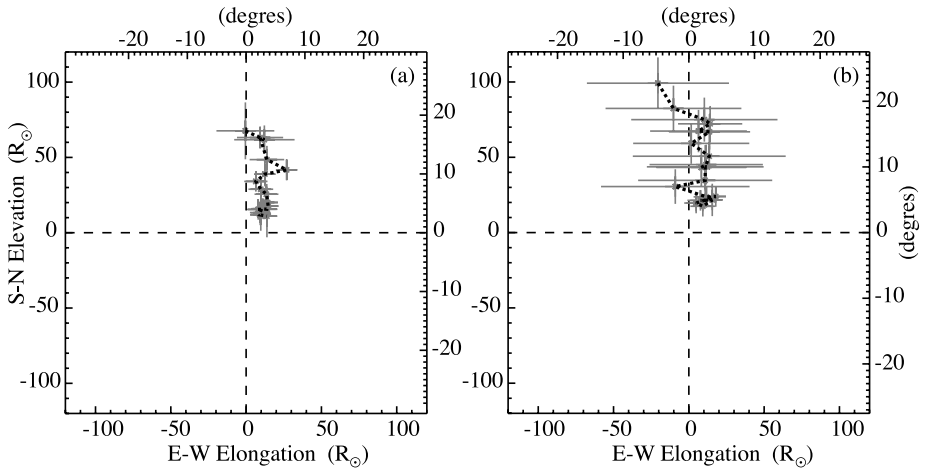

Fig. 5 Waves/RAD1 (**a**) and Cassini/RPWS/HFR (**b**) GP results of a solar type III radio burst observed simultaneously by the two spacecraft between 12:25 and 14:30 UT on September 1, 1999. The plots show the source positions as a function of elongation and elevation (in units of degrees and solar radii). The results are in good agreement with the type III source moving along northern Archimedean spiral-like magnetic field lines, consistent with the AR's location on the Sun

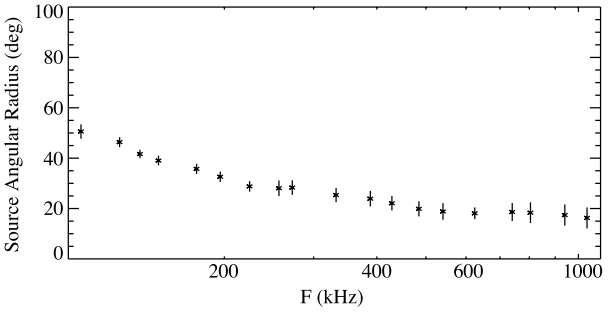

Fig. 6 Waves/RAD1 GP results of type III solar radio burst observed by Wind between 12:25 and 14:30 UT on September 1, 1999. The plot represents angular radius of the apparent source in degree as a function of frequency. Since the type III burst apparent source is extended, GP measurements which take account of the angular radius γ of the source will also be applied to S/Waves data

spacecraft are in good agreement. Moreover, we can check that above 200 kHz the Cassini and Wind goniopolarimetric results are giving the same direction of arrival.

5 Summary and Concluding Remarks

This paper has presented the different GP inversions available for space-borne radio receivers. Both spinning and stabilized spacecraft have been discussed. The GP specifics of the S/Waves instrument were presented in Sect. 3. We did not explicitly provide GP inversions or calibration inversions in this paper, but they are available in the various referenced papers. The GP inversion including the size of the source as a GP unknown is currently being developed and is the subject of a future paper.

In Sect. 4, we analyzed a type III burst observed with the Cassini and Wind radio receivers. We showed that both receivers provided the same source characteristics. However, as the Wind spacecraft is a spinning spacecraft, one spacecraft rotation (i.e., 3 sec) is necessary to obtain GP measurements. This also implies that the emission must remain constant

over a spacecraft spin. The GP measurement on the Cassini and STEREO receivers are only limited by the receiver integration time which is of the order of a few tens of milliseconds, depending on the instrument operating mode. When operating in an antenna switching mode (i.e., GP1 or GP2 modes), the time coherence of the source has to be greater than the time needed to switch antenna between successive GP0 measurements, which is a few tens of milliseconds. The S/Waves instrument is less sensitive than the Wind radio receivers to temporal variations of the observed signal. However, as Cassini and STEREO GP measurements include a smaller number of measurements than the Wind ones, the Cassini and STEREO GP results are then more sensitive to SNR errors.

The data coding used for S/Waves data is a significant improvement compared to the one used with the Cassini radio receiver. The S/Waves data are coded with 12-bit words, whereas the Cassini/RPWS/HFR data with 8 bits only. It has been showed that the digitization noise induced by 8-bit coding was the most important source of noise in the case of Cassini (Cecconi 2004; Cecconi and Zarka 2005). The new 12-bit coding reduces the digitization noise by a factor of $\sim$16 (i.e., the expected order of magnitude as $2^{12}/2^8 = 16$).

The error bars displayed for the GP results obtained from Cassini show that the choice of the instrument operating mode (integration time and frequency bandwidth, which are determining the measurement noise level) is essential to obtain the desired accuracy. As the S/Waves receivers include a more efficient data coding (12 bits instead of 8 bits), the recorded data will eventually be more accurate than Cassini/RPWS even with the same bandwidth and integration time.

Another improvement on STEREO, with respect to the Cassini radio receiver, is the shorter antenna used. This allows pushing up the high-frequency limit of quasi-static frequency range defined as $L \leq 10\lambda$. The monopoles are physically shorter (6 m for STEREO, 10 m for Cassini), but the effective lengths are also shorter in the case of STEREO: preliminary results from electromagnetic wire-grid simulations (Rucker et al. 2005; Oswald et al. 2006) give effective lengths of the order of 1.5 m, whereas the effective antenna length obtained for Cassini/RPWS/HFR is 1.68 m for the monopole antennas. The effective antenna length shall however be calibrated in-flight using the radio galactic background as a calibrated source.

Regarding type III observations, GP measurements provided by the new generation of receivers onboard stabilized spacecraft like Cassini or STEREO, offer great opportunities to study solar radio bursts with the best accuracy. It is then possible to retrieve radio source trajectories in the corona and the solar wind as well as to obtain the size and the possible polarization of the radio emissions.

Furthermore, in order to get accurate radio source locations in the corona and IPM, triangulation will be performed on GP measurements from the STEREO-A and -B spacecraft. This allows one to trace out Coronal Mass Ejections (CMEs) which drive shocks emitting type II radio bursts, as well as solar energetic electrons responsible for type III bursts. Propagation effects are both the main issues in solar radio burst studies, and their study will provide great a tool for sounding IPM properties. GP measurements applied on S/Waves will bring essential observational constraints on these propagation effects: joint observations of visible CMEs by the Sun Earth Connection Coronal Heliospheric Observatory (SECCHI; see Howard et al. 2007, this issue) and of associated type II radio burst emissions by S/Waves will provide, for the first time, CME trajectories in the IPM and comparison between optical observations and radio observations based on GP measurements.

Acknowledgements The authors wish to thank P.-L. Astier and M. Dekkali (LESIA, Observatoire de Paris, France) for their helpful comments and discussions. The Austrian team, lead by H.-O. Rucker (Austrian Academy of Sciences, Space Research Institute, Graz, Austria) is also thanked for its work on antenna modelling. They finally also thank Q.-N. Nguyen for her deep involvement in the processing of the S/Waves data.

References

S. Bale et al., Space Sci. Rev. (2007, this issue). doi:10.1007/s11214-007-9251-x
J.-L. Bougeret et al., Space Sci. Rev. (2007, this issue)
B. Cecconi, PhD thesis, Observatoire de Paris-Université Paris 7, Meudon, France, 2004
B. Cecconi, Radio Sci. **42**, RS2003 (2007)
B. Cecconi, P. Zarka, Radio Sci. **40**, RS3003 (2005)
G.A. Dulk, J.-L. Steinberg, S. Hoang, Astron. Astrophys. **141**, 30 (1984)
G.A. Dulk, J.L. Steinberg, S. Hoang, A. Lecacheux, in *The Sun and the Heliosphere in Three Dimensions*, ed. by R.G. Marsden. ASSL, vol. 123 (1986), p. 229
G.A. Dulk, W.C. Erickson, R. Manning, J.-L. Bougeret, Astrophys. J. **365**, 294 (2001)
J. Fainberg, R.G. Stone, Space Sci. Rev. **16**, 145 (1974)
J. Fainberg, S. Hoang, R. Manning, Astron. Astrophys. **153**, 145 (1985)
G. Fischer et al., in *Planetary Radio Emissions V*, ed. by H.O. Rucker, M.L. Kaiser, Y. Leblanc (Austrian Acad. of Sci. Press, Vienna, 2001), p. 347
D.A. Gurnett, M.M. Baumback, J. Rosenbauer, J. Geophys. Res. **83**, 616 (1978)
D.A. Gurnett et al., Space Sci. Rev. **114**, 395 (2004)
J. Hanasz, R. Schreiber, H. de Feraudy, M.M. Mogilevsky, T.V. Romantsova, Ann. Geophys. **16**, 1097 (1998a)
J. Hanasz et al., Cosm. Res. **36**, 575 (1998b)
J. Hanasz et al., J. Geophys. Res. **108**, 1408 (2003)
S. Hoang, G.A. Dulk, Y. Leblanc, Astron. Astrophys. **289**, 957 (1994)
S. Hoang, M. Maksimovic, J.-L. Bougeret, M.J. Reiner, M.L. Kaiser, Geophys. Res. Lett. **25**, 2497 (1998)
S. Howard et al., Space Sci. Rev. (2007, this issue)
M.L. Kaiser, Adv. Space Res. **36**, 1483 (2005)
P.J. Kellogg, Astron. Astrophys. **169**, 329 (1986)
J.D. Kraus, *Radio Astronomy* (McGraw-Hill, New York, 1966)
W.S. Kurth, M.M. Baumback, D.A. Gurnett, J. Geophys. Res. **80**, 2764 (1975)
H.P. Ladreiter, P. Zarka, A. Lecacheux, Planet. Space Sci. **42**, 919 (1994)
H.P. Ladreiter, P. Zarka, A. Lecacheux, W. Macher, H.O. Rucker, R. Manning, D.A. Gurnett, W.S. Kurth, Radio Sci. **30**, 1699 (1995)
A. Lecacheux, Astron. Astrophys. **70**, 701 (1978)
R. Manning, J. Fainberg, Space Sci. Inst. **5**, 161 (1980)
T. Oswald et al., in *Planetary Radio Emissions VI*, ed. by H.O. Rucker, W.S. Kurth, G. Mann (Austrian Acad. Sci. Press, Vienna, 2006), p. 475
M. Panchenko, Radio Sci. **39**, 6010 (2004)
M.J. Reiner, J. Fainberg, R.G. Stone, J. Geophys. Res. **98**, 18767 (1993)
M.J. Reiner, M.L. Kaiser, J. Fainberg, J.-L. Bougeret, R.G. Stone, Geophys. Res. Lett. **25**, 2493 (1998a)
M.J. Reiner, J. Fainberg, M.L. Kaiser, R.G. Stone, J. Geophys. Res. **103**, 1923 (1998b)
M.J. Reiner, M.L. Kaiser, J. Fainberg, R.G. Stone, J. Geophys. Res. **103**, 29651 (1998c)
M.J. Reiner, B.V. Jackson, D.F. Webb, D.R. Mizuno, M.L. Kaiser, J.-L. Bougeret, J. Geophys. Res. **110**, A09S14 (2005)
M.J. Reiner, M.L. Kaiser, J. Fainberg, J.-L. Bougeret, Sol. Phys. **234**, 301 (2006)
H.O. Rucker, W. Macher, R. Manning, H.P. Ladreiter, Radio Sci. **31**, 1299 (1996)
H.O. Rucker, W. Macher, G. Fischer, T. Oswald, J.-L. Bougeret, M.L. Kaiser, K. Goetz, Adv. Space Res. **36**, 1530 (2005)
J.-L. Steinberg, G.A. Dulk, S. Hoang, A. Lecacheux, M.G. Aubier, Astron. Astrophys. **140**, 39 (1984)
D.F. Vogl et al., J. Geophys. Res. **109**, A09S17 (2004)
P. Zarka, B. Cecconi, W.S. Kurth, J. Geophys. Res. **109**, A09S15 (2004)